Analysis of Algal Biofilms with Confocal IMS

ICORS 2010

Arc/Spark Optical Emission Spectrometers

Measuring Cellular-Scale Nutrient Distribution in Algal Biofilms with Synchrotron Confocal Infrared Microspectroscopy

Infrared microspectroscopy (IMS) and chemical imaging is ideal for measuring nutrient distribution in single algal cells on a cellular and subcellular level. To enable the study of small algal cells, or cells within a colony requires enhanced spatial resolution IMS. Synchrotron IMS with confocal image plane masking provides spatial resolution at the diffraction limit, which allows the study of microecological interactions with a minimum target width of ~5 µm. Many species that contribute substantially to ecosystem productivity and nutrient cycling require this optical advantage. This spatial resolution can also provide insight into physiological advantages of various algal growth forms. For example, it allows the measurement of individuals within a colony. We used synchrotron confocal IMS to measure the response of two dominant algal species from a stream biofilm to a reduction in nutrient availability: *Achnanthes affinis*, a single cell (5 × 10 µm) diatom, and *Fragilaria virescens*, a colonial diatom (5 × 50 µm cells connected lengthwise). Initially, both species had similar variation in relative nutritional pools, but had unique changes in their relative carbohydrate, phosphorous compound, and lipid concentrations over time. *F. virescens* individuals were more similar to others within the same colony than to individuals in other colonies. The response of *F. virescens* colonies varied with colony length, as long colonies had a stronger response than short colonies. Synchrotron IMS spatial resolution allows the biochemical analysis of smaller and more closely associated algae, and increases the ability to predict how algal communities will be affected by changing environmental conditions.

Justin N. Murdock, Walter K. Dodds, John A. Reffner, and David L. Wetzel

The microscope and infrared spectrometer are two of the most useful tools for the study of biological materials, and their combined analytical power far exceeds the sum of the two. Performing molecular spectroscopy through a microscope superimposes chemical information onto the physical microstructure obtained from the optical microscope when visible and infrared information are collected under the same conditions. The instrument developments that enable current infrared microspectroscopic studies began with the introduction of the first research-grade infrared microscope, patented in 1989 (1). By 1993, published reports using this method to determine macroalgae (seaweed) cell-wall composition appeared (2-4). Since these initial reports, the use of infrared microspectroscopy (IMS) in microalgal (single cells or groups of cells) research has grown. Primarily, cultured algae have been used to hone IMS methodology and evaluate its capabilities in algal research (5–8). Studies involving natural, mixed species assemblages, which can utilize the spatial resolution potential of this technique fully are rare (9–11). For instance, in a recent review of IMS microalgal ecological research (12), only 3 of the 29 peer-reviewed publications investigated natural algal assemblages. Both thermal and synchrotron infrared sources
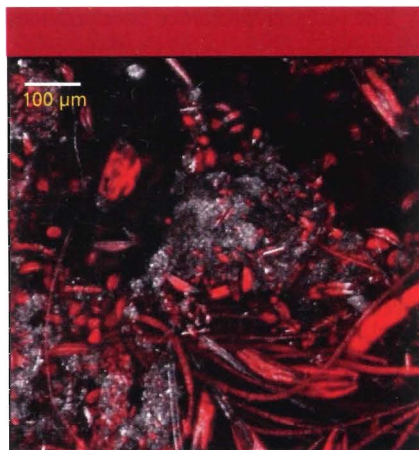
Figure 1: Micrograph of algal chlorophyll fluorescence (red) on a rock (white) collected with confocal laser scanning microscopy. Note the variety of cell shape configurations and sizes among the benthic algal species. Larger species and colonies are routinely analyzed by conventional IMS. The small size of many species (<10 μm) requires high spatial resolution to analyze individual cells.

provide a resolution capable of measuring individual algae in mixed species assemblages, and each has its advantages. For example, thermal source IMS is more accessible, allowing more samples to be analyzed than synchrotron IMS. However, synchrotron IMS with confocal masking provides superior resolution, which can be critical in isolating small or contiguous cells.

Algal ecology is the study of the interaction between algae and their environment. Infrared microspectroscopy addresses a major logistical problem in this field, obtaining species-specific cellular biochemical information from natural, mixed-species assemblages (11,12). Benthic (bottom-dwelling) algae, for example, grow in a three-dimensional matrix (biofilm) composed of different cell sizes, shapes, and configurations. The optical and ecological challenge of studying algae is apparent from Figure 1, which shows a photomicrograph of algal chlorophyll fluorescence on a rock. Several issues make it difficult to obtain single species measurements with standard techniques: cell sizes can vary over an order of magnitude; species can occur as single cells, long filaments, or globular colonies; a number of different species can be found within a few square millimeters; and fluorescence can vary

across cells (that is, the physiological state varies across cells).

Synchrotron IMS is a tool that can be used to begin to overcome these spatially related challenges by giving a species- and location-specific measurement of an individual alga's relative chemical composition and distribution. This technique enables algal ecologists to focus on new, ecologically relevant questions such as what level (that is, cell, colony, and population) best defines a species' response to environmental change. For instance, many species occur as single cells and thus can be measured as individual organisms. However, the variety of growth forms and sizes can make it difficult to define the best unit to measure multicellular groups in terms of its functional role such as primary productivity (that is, carbon incorporation) and nutrient cycling. Understanding how individual algal species within a diverse community respond to environmental changes can help predict how changes in assemblage structure will impact overall assemblage function.

Optical tools: Projected image plane masking of a front-surface Schwar-

zschild microscope objective focuses an infrared microbeam onto a visually selected target on the microscope stage. This optical arrangement accepts rays from the beamsplitter of an optically interfaced Fourier-transform infrared (FT-IR) spectrometer to provide localized spatial resolution of a few micrometers (13). This process enables cellular and subcellular chemical analysis from fundamental molecular vibrational spectra. Spectra are obtained from single targeted points, as a programmed sequence along a line, or in a raster scanned grid. From these data, individual spectra, organic functional group line maps, or 3-D chemical images may be produced. The resulting spectra, or groups of spectra, reveal the relative proportion of different chemical species within each location (pixel) of the image (14). Therefore, spatial and temporal changes in algal biochemistry can be measured in cells exposed to different environmental conditions or locations in a biofilm. Although production of large images is made convenient by the use of focal plane array detectors (15), image plane

masking is not possible with this optical arrangement, limiting the spatial resolution within the image. With focal plane arrays, the nominal image pixel size is quoted from projection of an individual detector element dimension back to the image plane.

Conventional (thermal source) IMS has been used successfully to study large cells and colonies (12,16). However, synchrotron confocal IMS is necessary to achieve an appropriate spatial resolution (< 10 μm) for smaller algal cells and much of the dynamics of individual cells within colonies (17). Synchrotron radiation, with its brightness, absence of thermal noise, and nondivergence, produces a narrow beam of minimal cross section that is minimally attenuated by confocal image plane masking. Confocal masking overcomes image fuzziness from the optical geometry imposed by the obscuration caused by the secondary mirror of the Schwarzschild optics and eliminates the spectral contribution of diffracted rays that sample an area larger than the projected spot size. The result is a sharp, well-defined image and a true spectrum of only the targeted small algal cell.

Ecological and industrial importance of algae: Algae have an increasing ecological and economical importance. Algae are often the dominant primary producers in lighted aquatic ecosystems and mediate fundamental system processes by transforming inorganic nutrients (that is, carbon, nitrogen, and phosphorus) into organic compounds. Because of this fundamental process, algae are a primary food source for many aquatic food webs, and are vital in sequestering and processing nutrients and pollutants that can cause ecological imbalances (18). Algae can be highly sensitive to chemical and physical environmental changes. Just as the well-being of a caged canary provides early warning of undesirable hazardous gases in a mine, changes in algal composition can be used as indicators of natural or anthropogenic pollution (19). Shifts in algal assemblages, often caused by humans' inputs into the environment, can be ecologically and economically detrimental (20). For example, increased nutrients can cause unsightly nuisance growth, decreased edible species, drink-ing water taste and odor problems, and increased algal toxin production (21). Understanding nutrient–algal relationships has led to the use of algal bioreactors and waste stabilization ponds to remove nutrients in advanced sewage treatment systems (22–24). The economic impact of algae is increasing rapidly. In the search for alternative renewable energy sources, algae-based biofuel has recently spawned numerous private, governmental, and university organizations focused on the mass culture of particular species that are best suited to produce oil (lipids), reproduce quickly, or have specific nutritional qualities (for example, National Renewable Energy Laboratory's Aquatic Species Program, 25–27), with billions of dollars currently being invested.

Application of synchrotron confocal IMS — Measuring the chemical variation and response of two algal species within a biofilm: Relative to the human-scale environment, algae live in a drastically different world governed by distinctly different physical and chemical forces (28,29). Nutrient movement can be quite variable inside biofilms, potentially altering the relationship of cell growth and overlying water nutrient concentrations. A major regulator of nutrient movement is a diffusion boundary layer that develops above surfaces in flowing waters. This boundary layer is a transition from the turbulent, eddy-dominated flow with fast nutrient transport above and laminar flow below, in which molecular diffusion dominates nutrient movement (30). In mature, thick algal biofilms, this boundary layer often bisects the biofilm, separating overstory cells above and understory cells below (31). Therefore, spatial location (relative to the boundary layer as well as competitors) may influence nutrient availability at micrometer scales (32). Limited diffusion of nutrients into biofilms from above and differential uptake ability among species has been proposed to create microscale nutrient heterogeneity that potentially can lead to species composition changes and biofilm succession. However, there is little direct data on nutritional content heterogeneity among single algal species (or individuals) in a biofilm to support these hypotheses.

The research presented here provides an example of the level of cellular compositional data that can be obtained with IMS and demonstrates its potential for advancing algal ecological studies. We used synchrotron confocal IMS to study the relative chemical changes among individuals of two algal species in a natural benthic algal assemblage following a reduction in nutrient (nitrogen and phosphorus) availability. Each species was the dominant diatom species in the lower and upper biofilm (that is, cells directly attached to the substrata and cells entangled within other algal filaments extending into the water column). It is difficult to measure the exact location of the diffusion boundary layer. We chose extreme vertical limits and assumed these points represent maximum differences in diffusion-turbulent molecular transport. Because the same species of diatom did not occur in both locations sampled, a direct comparison between a single species across habitats was not possible. Therefore, our analysis focused on detecting differences in relative chemical composition within individuals of each species, as well as changes in relative chemical composition over time in a reduced nutrient environment. Variation in relative cellular macromolecular pools (that is, carbohydrates, protein, and lipid) among individuals and over time was analyzed using principal component analysis (PCA). Lipid-to-protein (L/P) ratios were also measured to assess a response in nutrient availability.

Experimental

Algal specimen collection: A total of 10 infrared reflective glass slides (Mirr IR, Kevley Technologies, Chesterland, Ohio) were placed adjacent to one another in a large (1400-L) recirculating stream at the experimental stream facility of the Konza Prairie Biological Station near Manhattan, Kansas. Water nutrient concentrations were approximately 440 μg/L NO_3-N and 25 μg/L PO_4-P. Slides were removed from the stream after 7 days. This colonization time produced monolayer areas of cells intermixed with larger and thicker clumps of algae and detritus, as noted with visible examination of the slides. Additionally, 10 rocks from

within 0.5 m of the slides with an established (approximately 21 days old and several centimeters thick) algal biofilm were collected. Light and water velocity between colonized slides and rocks were similar. Immediately after removal from the stream, slides and rocks were randomly placed in a 22-L recirculating chamber under fluorescent plant grow lights (~350 µmol quanta/m^2 PAR) with a water velocity similar to that of the stream (~10 cm/s). The chamber was filled with low nutrient springwater and nitrate (1 mg of KNO_3 and phosphorus in a 16:1 molar ratio) was added to produce an initial chamber concentration of 227-µg/L NO_3-N and 20-µg/L PO_4-P (N:P = 16:1 by mole). One slide and one rock were removed from the chamber after 30, 180, and 360 min. A 6-h timeframe is likely shorter than benthic diatom cellular division rates, which can range from 6.5 h to 16 days (33,34), and likely minimized cell content dilution due to cell division. NO_3-N concentrations decreased linearly in the chamber over the 6 h from 227–215 µg/L.

Slides were air-dried immediately upon removal from the chamber and stored in a desiccator until IMS analysis. A single cell pennate diatom (*Achnanthes affinis*, ~5 µm × 10 µm cell size, Figure 2) was the dominant alga on slides. To prepare the loose overstory algae for IMS analysis, algal filaments were removed from the rock, rinsed with deionized water, and placed on an infrared reflective glass slide with a few drops of water. Algae were immediately spread apart with tweezers, air dried, and then placed in a desiccator. The dominant diatom in the overstory samples was a colonial pennate diatom (*Fragilaria virescens*, ~5 µm × 15 µm cell size) that formed chains of cells (ranging from ~5 to 50 cells per colony) attached side by side (Figure 2).

Infrared confocal microspectroscopy: IMS was conducted on beamline U10b at the National Synchrotron Light Source at Brookhaven National Laboratory, Upton, New York. This beamline was equipped with a Continµum IR microscope optically interfaced to a Magna 850 FT-IR spectrometer (Nicolet/Thermo, Madison, Wisconsin). Spec-
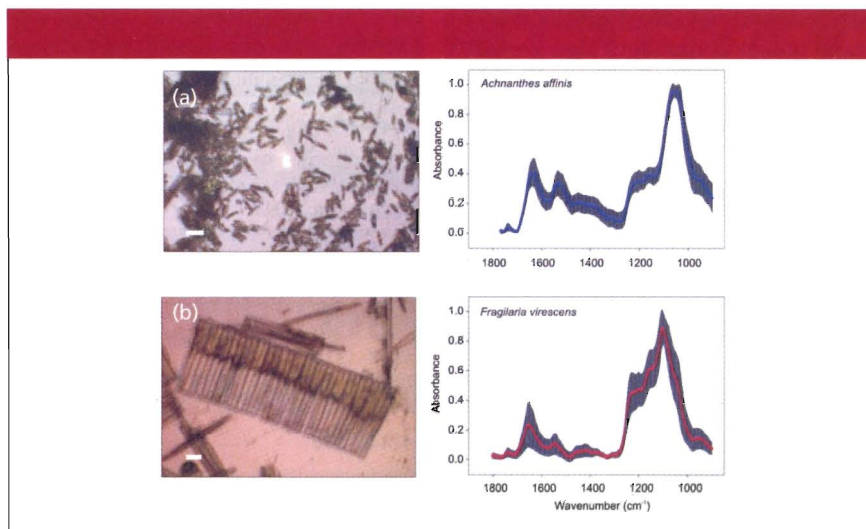

Figure 2: Micrograph of the diatoms (a) *Achnanthes affinis* and (b) *Fragilaria virescens*. Scale bars = 10 µm. Average spectra (color) and standard deviation (black outlines) of *A. affinis* (*n* = 180) and *F. virescens* (*n* = 617) for all individuals at all time points.

tra were taken in reflection–absorption mode with a resolution of 6 cm^{-1} and 128 scans coadded. Confocal 5 µm × 10 µm image plane masking was used for *A. affinis*, and the mask rotated so each cell filled the masked area. Spectra of 30 individual cells were collected without bias from the time-0 slide, and 50 cells from the 30-, 180-, and 360-min slides for a total of 180 individual spectra.

A line map was collected through *F. virescens* colonies with a 5 × 15 µm aperture. Line maps from seven colonies (87 total spectra) were collected from the control rock, and line maps of 10 colonies from the 3-h (214 total spectra) and 6-h (316 total spectra) rocks for a total of 617 individual spectra. During the drying process, cellular contents within diatoms typically condensed and shifted toward one region of the cell (see Figure 2). Line maps were collected through these regions containing the cellular material in 4–5-µm increments resulting in approximately one spectrum for each cell in the colony. Differential movement of organic material during dehydration could have occurred, underestimating some cellular components in the line maps; however, spectra collected from regions of the cell not containing visible cellular material had little absorption other than the silica band.

Spectral analyses and band assignments: Relative cell nutrient content and heterogeneity among *A. affinis* and

F. virescens individuals were measured using the 1800–900 cm^{-1} region, which contains the majority of the distinguishing information in algae (that is, carbohydrates, protein, lipid, and phosphorylated compounds [5,17]). Lipid-to-protein ratios, which can show a strong change due to altered nutrient availability (6,35,36), were also quantified as an additional measure of cellular allocation changes in response to a changing environment. All spectra were manually baseline corrected and normalized to the maximum absorbance value (the silica peak) before analysis using OMNIC 7.4 (Thermo Scientific, Waltham, Massachusetts). A strong silica band from the diatom's cell wall was observed at ~1035 cm^{-1} and 1100 cm^{-1} for *A. affinis* and *F. virescens*, respectively. Although these silica bands fell within the range of reported values, it is unclear why they differed between these two species. Ratios of lipid (ester carbonyl at 1740 cm^{-1}) to protein (amide I at 1650 cm^{-1}) were measured by comparing peak area ratios calculated from the integrated areas under each peak using the peak area function in OMNIC 7.4.

Macromolecular variation among individuals and over time was assessed using separate PCAs for each species. For each PCA, all spectra from a species (1800–900 cm^{-1} region) at all time points were included, and varimax rotation of principal component

applied (Unscrambler 9.8, Camo Software Inc, Woodbridge, New Jersey). Loading plots of principal components showed which macromolecules had the greatest variation within and among time points. Lipid-to-protein ratio variability in individuals over time was compared with a Levene's test. A repeated-measures analysis of variance (RM-ANOVA) compared temporal changes in L/P ratios among *A. affinis* individuals. Kendall's W nonparametric test was used to test L/P variation in *F. virescens* due to inconsistent variance among time points. Additionally, L/P ratio dynamics within and among colonies of *F. virescens* were assessed to determine how individual cell nutrient distribution varied within colonies and if cell response to changing nutrients was related to colony size. Band assignments were based on band assignment from the available FT-IR algae literature and are listed in Table I.

Results

Relative nutrient variation among individuals: Cellular nutrient distribution among individuals was similar in both species. The majority of variation among cells was due to carbohydrates, which explained 38% and 47% of the variation in *A. affinis* and *F. virescens* respectively. Proteins (amide I and II) explained 22% of the variation of cellular content in both species. Specifically, spectral variation among *A. affinis* individuals was predominantly due to carbohydrate bands from 1020–928 cm^{-1} (C-O-C, PC2, 26%) and 1200–1060 cm^{-1} (C-O-C stretch, PC3, 12%, Figures 3a–3c). Protein peaks at 1634 (C-O stretch) and 1543 cm^{-1} (combination of N-H bend and C-N stretch, PC4, 22%), and from 1489–1313 cm^{-1} (CH$_3$ and CH$_2$ bend of proteins and amide III region, PC1, 18%) also contributed substantially to cellular variation. *A. affinis* individuals also noticeably differed in the phosphodiester region at 1244 cm^{-1} (P=O, PC5 5%), and a possible polyphosphate (P-O-P, 980–940 cm^{-1}) contribution to the 1020–928 cm^{-1} band in PC2. *Fragilaria virescens* individuals differed most in the carbohydrate region from 1200-1115 cm^{-1} (C-O stretch, PC1, 24%, Figures 4a–4c) and at 1038 cm^{-1} (PC3,

Table I: FT-IR band assignments for algal functional groups

Wavenumber Range (cm^{-1})	Band Assignment	Functional Groups
1745–1734	v C=O of esters	Membrane lipids, fatty acids
1720–1700	v C=O of esters	Carboxylic group of esters
1655–1638	v C=O	Protein (Amide I)
1545–1540	δ N-H, v C-N	Protein (Amide II)
1456–1450	δas CH$_2$, δas CH$_3$	Lipid, protein
1460–1392	δ C-O	Carboxylic group
1398–1370	δ CH$_3$, δ CH$_2$/δ C-O	Proteins, carboxylic groups
1320	v C-H, δ N-H	Proteins
1244–1230	vas P=O	Nucleic acids, phosphoryl group
1200–900	v C-O-C/vas P=O	Polysaccharides/nucleic acid
1150–1000	v C-O/v Si-O	Polysaccharides/siloxane
1090–1030	v P=O	Nucleic acids
1090–1020	v Si-O	Siloxane
980–940	P-O-P	Polyphosphate
950	v Si-H/v Si-OH	Silane/silanol

v = symmetric stretch, vas = asymmetric stretch, δ = symmetric deformation (bend), δas = asymmetric deformation (bend)
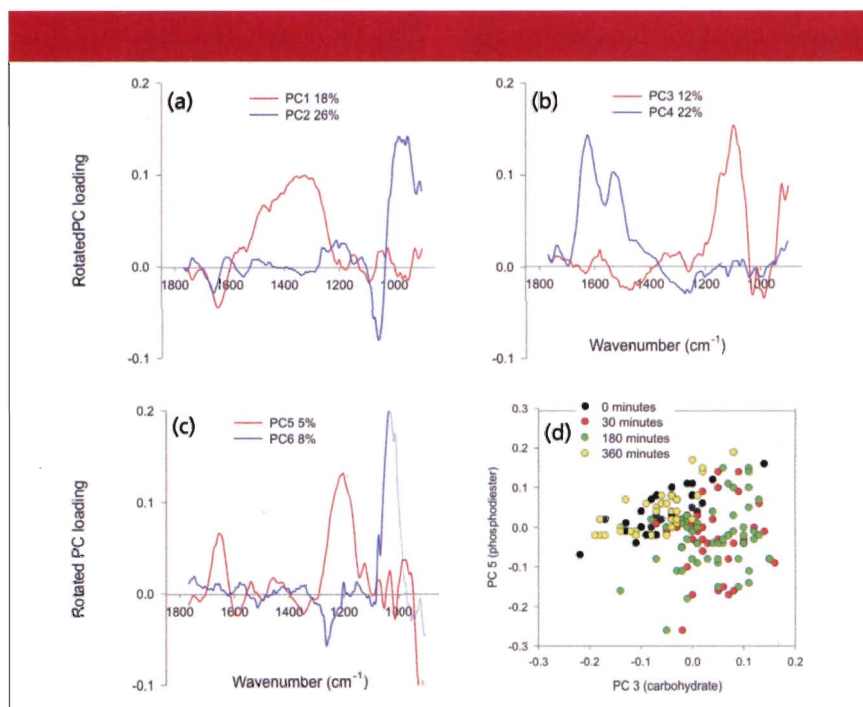Band assignments were taken from references 27 and 41–44.

Figure 3: (a–c) Rotated PCA loading plots of *Achnanthes affinis* spectra (1800–900 cm-1). (d) PCA biplot of the PC3 and PC5 (the factors with the strongest temporal shift — that is, carbohydrates and phosphodiesters). Temporal shift was temporary and cell contents at 360 min are similar to initial values.

23%), and in protein bands at 1659 and 1554 cm^{-1} (PC2, 22%). Spectral variation was also observed in *F. virescens* in the phosphodiester peak at 1244 cm^{-1} (PC5, 13%).

Temporal response: Both *A. affinis* and *F. virescens* showed a measurable change in relative nutrient distribution in chambers relatively quickly (within 30 min), however this change appeared
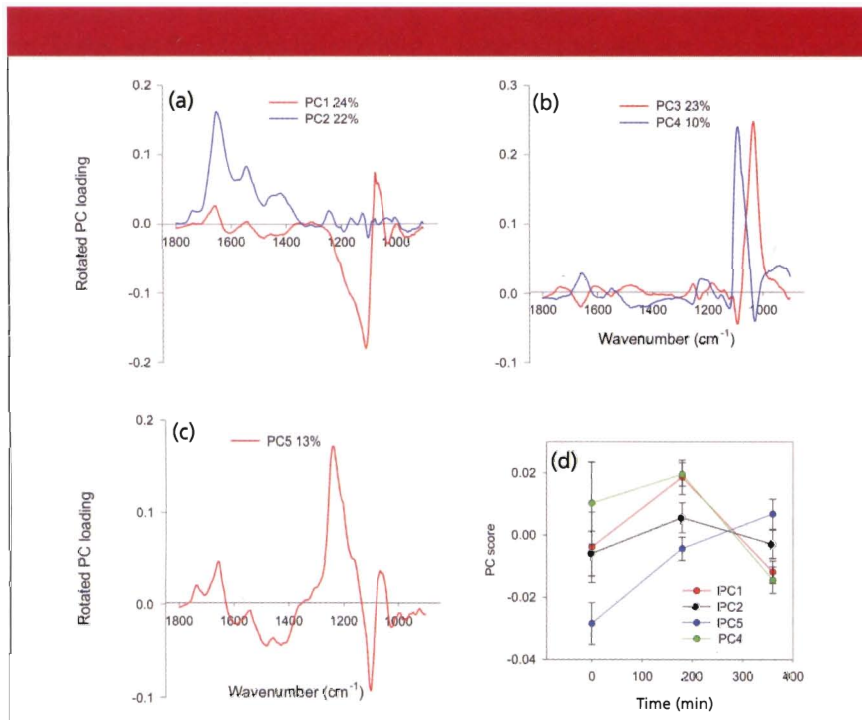
Figure 4: (a–c) Rotated PCA loading plots of *Fragilaria virescens* spectra (1800–900 cm^{-1}). (d) Change in PC scores over time for PC1 (carbohydrate), PC2 (protein), PC4 (carbohydrate), and PC5 (phosphodiester). Error bars are 95% confidence intervals.

temporary, shifting back toward initial relative nutrient distributions by 360 min. The two diatoms had slightly different chemical trajectories. For example, temporal changes in *A. affinis* were dominated by increasing then decreasing relative carbohydrates (PC3), and decreasing then increasing relative phosphodiester content (PC5, Figure 3d). The most prominent temporal shifts in *F. virescens* were decreasing then increasing relative carbohydrates (PC1), and increasing then decreasing relative protein content (PC2). However, relative phosphodiester content consistently increased over time in *F. virescens* (PC5, Figure 4d).

Lipid- to-protein ratios: Significant changes in L/P ratios were observed over time within each species. *A. affinis*' L/P ratio increased asymptotically over 360 min (means of 0.023, 0.035, 0.048, 0.058, for 0, 30, 180, and 360 min, respectively), with a significant increase by 180 min (RM-ANOVA, F3, 159 = 11.05, P < 0.001, Figure 5). There was an increasing trend in ratio variability among *A. affinis* cells with time (SD 0 = 0.011, 0.5 = 0.023, 3 = 0.024, 6 = 0.040), but this trend was only marginally significant (Levene's

test, P = 0.11). L/P ratios in *F. virescens* individuals increased linearly over 360 min (means of 0.019, 0.045, 0.073 for 0, 180, and 360 min, respectively, Kendall's W=0.335, Chi-square = 31.4, d.f. = 2, P < 0.001, Figure 5). Ratios variability among individuals over time was smaller than in *A. affinis*, but had significantly increased by 360 min (SD = 0.017, 0.015, 0.021, Levene's test, P < 0.001).

Colony dynamics: Colony nutrient variation: Synchrotron IMS allowed the measurement of individual cells in *F. virescens* colonies, providing intra- and intercolony comparisons of nutrient distribution. Relative nutrient distribution was more similar within colonies than among colonies. For example, Figure 6 shows a spectral line map of a 15-µm wide transect through one colony at each time point (1800–750 cm^{-1}, normalized to the silica band). The variation in the protein (~1650 cm^{-1}), phosphodiester (1244 cm^{-1}), and carbohydrate (1200–1100 cm^{-1}) regions are visually more similar along the colony length than among colonies. Principal component analysis also showed variation in relative protein, carbohydrate, and phosphodiester content was substantially greater
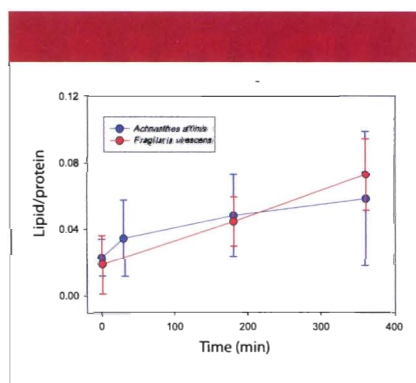
Figure 5: Lipid-to-protein ratios over time of *Achnanthes affinis* and *Fragilaria virescens* exposed to nutrient-depleted conditions. Error bars are one standard deviation.
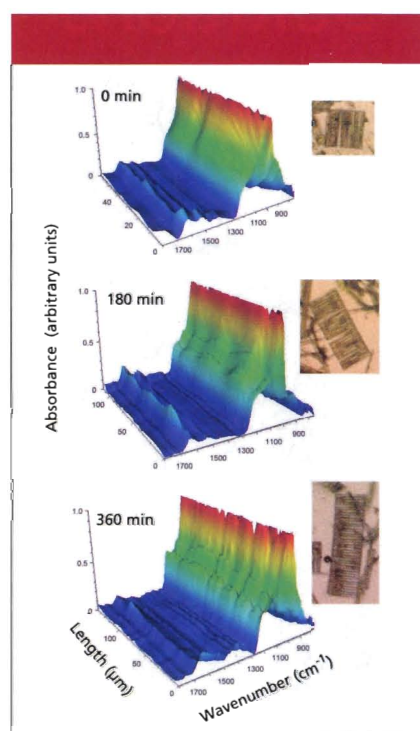

Figure 6: Spectral maps (1800-750 cm⁻¹) of 5-μm increment line transects through three representative *Fragilaria virescens* colonies at (a) 0, (b) 180, and (c) 360 min. Spectra were normalized to the silica peak.

among colonies than within a colony at all time periods (Figure 7, PC biplots at 0, 180 and 360 min). Additionally, individual cell L/P ratios were more similar within than among colonies at times 0 (ANOVA F1.45= 6.15, P= 0.017) and 360 min (ANOVA F1, 352 = 20.6, P < 0.001), but not at 180 min.

Influence of colony size: Colony size (the number of individuals attached together) was correlated to colony re-

sponse. *Fragilaria virescens* colonies occurred in a large range of sizes (2 to over 200 individuals per colony) with a visual median estimate of 10–30 individuals (50–150 μm) per colony. Colonies of different sizes occurred at the same location in the biofilm. The relationship between colony L/P ratio and colony size changed over time. Initially, ratios decreased with increasing colony length, as longer colonies had higher relative protein content. After 180 min, there was no relationship, and then ratios increased with increasing colony length at 360 min (Figures 8a–8c). This trend was driven by a larger change in L/P ratios in longer colonies, and similar L/P ratios among individuals in a colony, regardless of cell location in the colony (that is, end versus middle, Figure 6, Figures 8d–8f). From 180 to 360 min, mean L/P ratios of colonies greater than 100 μm roughly doubled from 0.04 to 0.08, whereas mean ratios in colonies shorter than 100 μm decreased from 0.05 to 0.04. As L/P ratios increased in long colonies, variation in this ratio among cells in the same colony also increased (that is, SD of 0.007 versus 0.011 for 180 and 360 min, respectively).

Discussion

Synchrotron confocal IMS detected the relative macromolecular variation among small single-cell algae and among individuals within a colony, as well as a consistent short-term (hours) change in chemical distribution (L/P ratios). Despite a substantial difference in cell size, growth form, and location in the biofilm, both diatom species varied mainly in relative carbohydrate and protein content. A change in carbohydrates and proteins in these two species is consistent with community-scale (that is, whole biofilm) nutrient variation observed in benthic algae assemblages under nutrient limitation (37). In diatoms, energy storage products such as chrysolaminaran, and chloroplast pigments such as carotenoids are often major reservoirs of carbohydrates. Proteins generally are found in photosynthetic pigments such as chlorophyll a and c, nucleic acids, and a variety of amino acids (38). *A. affinis* also showed considerable variation from 980 to 920

cm⁻¹, the region that encompasses the vibration of polyphosphates. Algae can undergo excess "luxury" P consumption when nitrogen and carbon are limiting, and store P as insoluble polyphosphate granules for later conversion to energy (39). Spectral variation in these cellular components in both species suggests nutrient heterogeneity can be great enough in biofilms to produce measureable and meaningful differences in algal physiology at millimeter distances.

The principal components that explained the most variation in algal spectra did not show strong temporal trends. However, temporal changes were evident, showing that smaller, but still relevant variation can be detected in the presence of larger cell-to-cell nutrient heterogeneity. In *A. affinis*, temporal (albeit inconsistent) changes were found in decreasing then increasing proportions of carbohydrates and phosphodiesters (PC3 and PC5, 17% combined explained variance), suggesting that although overall cell nutrient distribution was not greatly affected, changes were indeed occurring. In *F. virescens*, phosphodiester proportions (PC5, 13%) consistently increased over time as carbohydrate proportions decreased and then increased back to initial values. The 6-h timeframe of this study was used to limit cellular nutrient changes due to cell division, but this short time also likely limited a large shift in the major pools that have been noted in other IMS algal research on diatoms (40,41). However, the direction of chemical changes in both species was consistent with other IMS studies. For example, diatoms have been shown to reduce relative protein and carbohydrates and increase relative lipids during nitrogen limitation experiments (6). Diatoms also can reduce phosphodiester content in relation to lipid and carbohydrate content while experiencing phosphorus limitation (9).

A consistent trend among previous algal research is an increase in relative lipid content with cell stress, and a decrease in protein content with nitrogen limitation (6,8,9,17,40). In comparison to protein variation (amide I and II), lipid (C=O ester carbonyl at ~1740 cm⁻¹) was not a major factor differentiating spectra of individuals in either species; thus, variation in carbon allocation to oil stor-
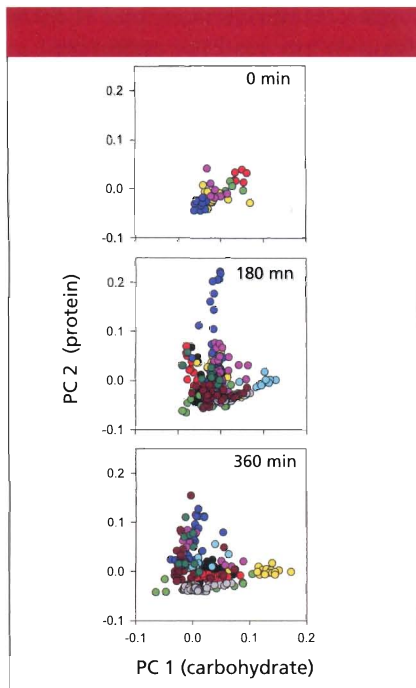
Figure 7: Temporal biplots of PC1 and PC2 (carbohydrate and protein) for 0, 180 and 360 min. In each biplot, circles of the same color are individuals within the same colony. Note that individuals within a colony grouped together at all time periods, suggesting that nutrient content was more similar within than among colonies and that changes in *Fragilaria virescens* nutrient distribution occurred at the colony rather than individual level.

Figure 8: *Fragilaria virescens* L/P ratio relationship with colony length after (a) 0, (b) 180, and (c) 360 min in nutrient-depleted conditions. Error bars are one standard deviation. (d–f) Relationship between L/P ratios of individual cells and a cell's location from the end of a colony at (d) 0, (e) 180, and (f) 360 min.

age products was likely small compared with carbohydrate synthesis. However, an increasing L/P ratio was observed in both species despite a high initial variation in macromolecular pools within each species. L/P ratios in both species increased at a similar rate, but *F. virescens* ratios did not plateau after 360 min, suggesting a greater overall change is possible in *F. virescens*. Regardless of their initial state, cells started and consistently increased their lipid-to-protein content over time, which is consistent with nitrogen limitation.

Colony Response to Changing Conditions: Defining the relative nutrient content of individuals within a colony and single, whole colonies of *F. virescens* provided new insight on how colonies of microorganisms respond to changing nutrient availability. Colonies developed in an artificial stream channel and were collected from rocks that were only centimeters apart. Thus, we assumed that
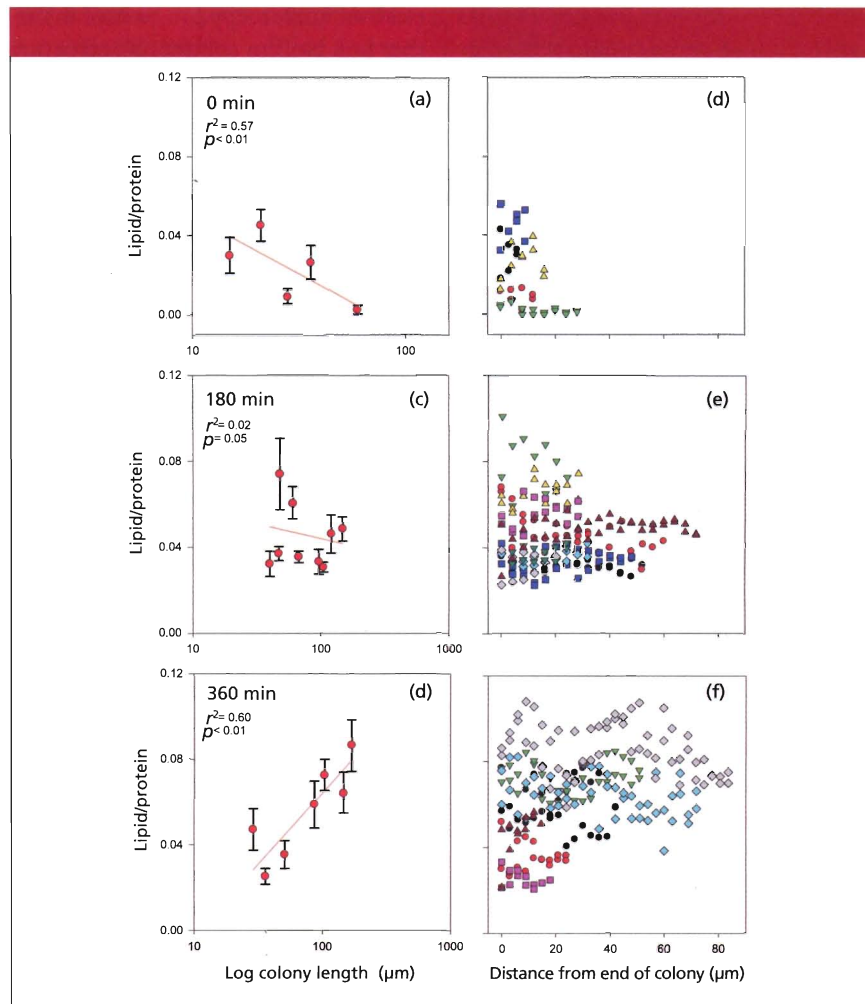
they developed in similar light, nutrient, temperature, and channel water velocity. The nutritional pattern of *F. virescens* colonies (individuals more similar within a colony than among colonies) suggests that colonies maybe were experiencing different nutrient availability within the biofilm and this difference was strong enough to cause distinct macromolecular changes. Colony relative nutrient content however, was strongly affected by its length, with longer colonies (> ~100 µm, 20 cells) showing a greater increase in L/P ratios over time.

Although this data provided new insight on how colonies respond to changing conditions, it also raised additional questions, and provided direction for further studies. For example, it

is difficult to determine if this quicker response in larger colonies is beneficial to the species' overall growth. In terms of present growth and reproduction, this fast physiological response harms the colony as carbon is switched to maintenance and survival products (lipids) and away from growth and reproduction (that is, protein). On the other hand, if conditions are deteriorating rapidly, an early start at "gathering food for the winter" can increase colony chances for longer-term survival until conditions improve. Because being large typically provides a positive effect to algae by becoming more resistant to being eaten (42), an overall negative growth effect associated with large colony size might help explain why all *F. virescens* are not found in large colonies.

It is not clear why longer colonies had a quicker response than shorter colonies. Visibly, there was no consistent difference among cells along a colony, or among colonies of different length. A decreasing surface area-to-volume ratio as cells join together can decrease an algal colony's nutrient uptake ability (43). However, the side-by-side organizational structure of *F. virescens* maintains a relatively consistent surface area-to-volume ratio (~90% of a single cell) with increasing length after three cells join together. Additionally, empirical nutrient mass transfer measurements near individual colonies of *Phaeocytis* (a spherical green algal colony) suggest that any diffusion boundary layer around colonies created by increased nutrient demand is not likely great enough to limit cell growth (44). Larger colonies of another alga (the green alga *Scenedesmus acutus*) had no change in photosynthetic efficiency or growth rates than smaller colonies (45). Diatoms might have differential responses to nutrients at the colony level. Increasing length makes it more likely that opposite ends may experience different micronutrient environments, but there was not a strong gradient in L/P ratio from one side to another, or from the periphery to the center cells (Figures 8d–8f). Perhaps shorter colonies are able to remain attached to the substrata in greater water velocities. Additionally, physiological measurements such as growth and nutrient uptake rates are needed to further address this question.

Synchrotron IMS as a tool in algal ecology: The spatial resolution provided by synchrotron confocal IMS allows the direct comparison of individual algae physiology with other nearby individuals, much the same as a fish ecologist would catch and assess individual fish in a lake or a botanist would monitor individual trees in a forest. Thus, IMS contributes greatly to algal ecology by making accessible a scale of interactions that is particularly relevant to these microorganisms (<10 μm), but has been difficult to measure directly. Adding individual cell chemical measurements to established microscopy techniques such as light, confocal laser scanning, and electron microscopy can be used to further link biofilm community structure to its potential response to environmental change. For example, the thickness or species composition of a biofilm can be better related to its ability to remove specific nutrients from overlying water.

The major benefit of IMS is the ability to measure changes in individual algae taken from natural assemblages combined with the ability to incorporate spatial distinction in nutrient distribution data. This involves optically cherry-picking individuals from a mass of closely associated species. Light microscopy can accurately elucidate assemblage structural change, but it does not detect the cellular chemical response that may lead to altered algal assemblages. Also, while spectroscopic analysis of biofilm "pellets" can provide valuable chemical information on algal assemblages, it is limited to assembly-averaged data.

Centuries of studying the ecological interactions of larger organisms have shown that intra- and interspecies interactions are strong regulators of community structure and function. As we learn more about the world of microbes, we see many similarities and differences in cell structure, metabolic pathways, and organism interactions compared with larger organisms. Many more microorganism species and forms can be investigated with the addition of synchrotron IMS and confocal image plane masking. By being able to predict how each species responds to unique external nutrient conditions, we can form a basis from which to predict how algal communities will shift given changes in nutrient loadings into a system and possibly predict under what conditions, and when algal blooms (including blooms of toxin producing species) will occur.

Acknowledgments

References

(1) R.G. Messerschmidt and D.W. Sting, U.S. Patent 4,877,960 (1989).

2) M. Sekkal, P. Legrand, J.P. Huvenne, and M.C. Verdus, *J. Mol. Struct.* **294**, 227–230 (1993).

(3) M. Sekkal, C. Declerck, J.P. Huvenne, P. Legrand, B. Sombret, and M.C. Verdus, *Mikrochim. Acta* **112**, 11–18 (1993).

(4) M. Sekkal, J.P. Huvenne, P. Legrand, B. Sombret, J.C. Mollet, A. Mouradigivernaud, and M.C. Verdus, *Mikrochim. Acta* **112** 1–10 (1993).

(5) M. Kansiz,, P. Heraud, B. Wood, F. Burden, J. Beardall, and D. McNaughton, *Phytochemistry* **52**, 407–417 (1999).

(6) M. Giordano, M. Kansiz, P. Heraud, J. Beardall, B. Wood, and D. McNaughton, *J. Phycol.* **37**, 271–279 (2001).

(7) L.G. Benning, V.R. Phoenix, N. Yee, and K.O. Konhauser, Geochim. *Cosmochim. Acta* **68**, 743–757 (2004).

(8) P. Heraud, B.R. Wood, M.J. Tobin, J. Beardall, and D. McNaughton, *FEMS Microbiol. Lett.* **249**, 219–225 (2005).

(9) J. Beardall et al., *Aquat. Sci.* **63**, 107–121 (2001).

(10) D.C. Sigee, A. Dean, E. Levado, and M.J. Tobin, *J. Phycol.* **37**, 19–26 (2002).

(11) J.N. Murdock, W.K. Dodds, and D.L. Wetzel, *Vib. Spectrosc.* **48**, 179–188 (2008).

(12) J.N. Murdock and D.L. Wetzel, *Appl. Spectrosc. Rev.* **44**, 335–361 (2009).

(13) D.L. Wetzel and S.M. LeVine, *Spectroscopy* **48**(4), 40–45 (1993).

(14) D.L. Wetzel, *Food Flavors: Generation, Analysis, and Process Influence* (Elsevier, Amsterdam, 1995).

(15) E.N. Lewis et al., *Anal. Chem.* **67**, 3377–3381 (1995).

(16) S.A. Patel, F. Currie, N. Thakker, and R. Goodacre, *R. Analyst* **133**, 1707–1713 (2008).

(17) P. Heraud, S. Stojkovic, J. Beardall, D. McNaughton, and B.R. Wood, *J. Phycol.* **44**, 1335–1339 (2008).

(18) H.B.N. Hynes, *The Biology of Polluted Waters* (Liverpool Univ. Press, 1960).

(19) R.L. Lowe and Y. Pan, *Algal Ecology: Freshwater Benthic Ecosystems* (Academic Press, San Diego, 1996).

(20) W.K. Dodds, W.W. Bouska, J.L. Eitzmann, T.J. Pilger, K.L. Pitts, A.J. Riley, J.T. Schloesser, and D.J. Thornbrugh, *Environ. Sci. Technol.* **43**, 12–19 (2009).

(21) W.K. Dodds, *Freshwater Ecology: Concepts and Environmental Applications* (Academic Press, San Diego, 2002).

(22) R.J. Craggs, W.H. Adey, K.R. Jenson, M.S. St. John, F. B. Green, and W.J. Oswald, *Water Sci. Technol.* **3**, 191–198 (1996).

(23) C. Pizarro, W. Mulbry, D. Blersch, and P. Kangas, *Ecol. Eng.* **26**, 321–327 (2006).

(24) A.N. Shilton, N. Powell, D.D. Mara, and R. Craggs, *Water Sci. Technol.* **58**, 253–258 (2008).

(25) J. Sheehan, T. Dunahay, J. Benemann, and P. Roessler, *A Look Back at the U.S. Department of Energy's Aquatic Species Program- Biodiesel from Algae* (National Renewable Energy Laboratory, Golden, 1998).

(26) J. Gressel, *Plant Sci.* **174**, 246–263 (2008).

(27) Q. Hu, M. Sommerfeld, E. Jarvis, M. Ghirardi, M. Posewitz, M. Seibert, and A. Darzins, *Plant J.* **54**, 621–639 (2008).

(28) B.B. Jørgenson, *The Benthic Boundary Layer* (Oxford University Press, Oxford, 2001).

(29) J.N. Murdock and W.K. Dodds, *J. Phycol.* **43**, 449–460 (2007).

(30) S. Vogel, *Life in Moving Fluids*, 2nd ed. (Princeton University Press, Princeton, 1994).

(31) W.K. Dodds and B.J.F. Biggs, *J. N. Am. Benthol. Soc.* **21**, 2–15 (2002).

(32) W.K. Dodds, *Appl. Environ. Microbiol.* **55**, 882–886 (1989).

(33) N. Tanaka, *B. Jpn. Soc. Sci. Fish.* **50**, 969–972 (1984).

(34) S. Morin, M. Coste, and F. Delmas, *Hydrobiologia* **614**, 285–297 (2008).

(35) D.C. Sigee, F. Bahram, B. Estrada, R.E. Webster, and A.P. Dean, *Phycologia* **46**, 583 (2007).

(36) A.P. Dean, J.M. Nicholson, and D.C. Sigee, *Eur. J. Phycol.* **43**, 345–354. (2008).

(37) P.L.M. Cook, B. Veuger, S. Böer, and J.J. Middelburg, *Aquat. Microb. Ecol.* **49**, 165–180 (2007).

(38) R. Patrick and C.W. Reimer, *The Diatoms of the United States, Exclusive of Alaska and Hawaii,* Vol. 1, (Academy of Natural Sciences of Philadelphia, Philadelphia, 1966).

(39) R.G. Wetzel, *Limnology*, 3rd ed. (Academic Press, San Diego, 2001).

(40) K. Stehfest, J. Toepel, and C. Wilhelm, *Plant Physiol. Biochem.* **43**, 717–726 (2005).

(41) Y. Liang, J. Beardall, and P. Heraud, *Botanica Marina* **49,** 165–173 (2006).

(42) W. Lampert, K.O. Rothhaupt, and E. von Elert, *Limnol. Oceanogr.* **39**, 1543–1550 (1994).

(43) J.P. Grover, *J. Phycol.* **25**, 402–405 (1989).

(44) H. Ploug, W. Stole, E.H.G. Epping, and B.B. Jorgensen, *Limnol. Oceanogr.* **44**, 1949–1958 (1999).

(45) M. Lürling and E. Van Donk, *Oikos* **88**, 111–118 (2000).

(46) S. Vardy and P. Uwins, *Appl. Spectrosc.* **56**, 1545–1548 (2002).

(47) A.P. Dean, M.C. Martin, and D.C. Sigee, *Phycologia* **46**, 151–159 (2007).

(48) A. Chiovitti et al., *Soft Matter* **4**, 811–820 (2008).

Justin N. Murdock is with Kansas State University, Manhattan, Kansas, and the USDA, Oxford, Mississippi. **Walter Dodds** is with Kansas State University, **John A. Reffner** is with John Jay College of Criminal Justice, New York, and **David Wetzel** is with Kansas State University. Please direct correspondence to: dwetzel@ksu.edu ∎